Drag and lift on rotating vanes in granular beds

Raenell Soller and Stephan A. Koehler*
Department of Physics, Emory University, Atlanta, Georgia 30322, USA
(Received 7 January 2006; revised manuscript received 27 April 2006; published 22 August 2006)

We have performed systematic experiments on vane intruders of different sizes and aspect ratios that are immersed and slowly rotated in beds of monodisperse glass beads of different diameters. We find that the torque and lift force on the vane increase with bead size. The measured torque on the rotating vanes follows a scaling behavior that depends on the effective immersion depth and the effective vane diameter. The torque increases with the square of the effective immersion depth and the square of the effective vane diameter, and closely resembles the scaling behavior previously reported for the torque on rotating cylinders. We also find that the vertical lift forces have a supralinear dependence on the effective immersion depth, and qualitatively resemble the plunging forces produced when an intruder is slowly immersed into beds of glass beads.

DOI: 10.1103/PhysRevE.74.021305 PACS number(s): 81.05.Rm, 83.10.Pp, 83.10.Bb

I. INTRODUCTION

Moving an intruder through granular matter is a common industrial process for mixing as well as the prevention of jamming and arching in granular flows. Many different types of experiments probing different aspects of intruder motion have been performed, such as intruders inserted in hopper flows [1,2], moving through granular beds [3–10], rotating intruders commonly known as Couette geometries [11,12], and impeller geometries for mixing [13,14]. These investigations have concentrated on force measurements in the direction of motion, which we call the drag force. However, forces orthogonal to the main direction of motion also occur [3], and have received far less attention although they can be considerable.

Early experiments on vertical posts partially immersed in rotating beds of sand were performed by Wieghardt, where the drag forces increased with immersion depth and post diameter, and depended weakly on the translational velocity [3]. Albert *et al.* [4,5] performed similar experiments at much slower velocities and with glass beads that were presheared by a granular comb in front of the vertical post [15]. They found that the mean drag forces were independent of the velocity for small velocities (less than a few mm/s). A simple scaling dependence of the drag force on the post diameter D and immersion depth Z was determined: $F \propto \rho g D Z^2$. They explained the parabolic dependence of the force on the post's immersion depth in terms of the mean granular pressure on the post, where the granular pressure increases linearly with depth. They also reported that the bead diameter had a negligible influence on the mean drag force. Zhou *et al.* [8,9] measured the drag forces on cylinders translating in confined beds of aluminum oxide granules, and reported results similar to those of Albert *et al.*; the drag forces were independent of velocity and proportional to rod diameter. However, Zhou *et al.* also found that the drag forces increased with the particle size, which in part was attributed to the aspherical shape of the granules.

Chehata, Zenit, and Wassgren performed experiments on cylinders inserted into slow, dense hopper flows using glass beads [1]. The drag force was found to increase linearly with the granular pressure, post diameter, and post length, which was in general agreement with the translating post measurements by Albert *et al.* [4,5]. However, they found that the drag force depended on the bead size, and in their data analysis introduced an effective post diameter, which was the sum of the post and bead diameter $D+d$.

The rotational drag, i.e., torque, on cylinders slowly rotating in granular beds has been investigated by several groups. Tardos *et al.* [11,12] performed experiments with powders, and found that in the slow regime, the torque was independent of the rotational velocity and bead size. The torque measurements also had a parabolic depth dependence and followed a simple scaling behavior $\tau \sim \rho g D^2 Z^2$. Bocquet *et al.* also performed experiments on rotating cylinders, and found a similar trend [16,17]. Both groups interpreted their results using continuum theories.

A consistent picture for the drag on cylinders either slowly translating or rotating in granular matter emerges from these studies. The drag force is related to the mean granular pressure on the cylinder, which in the case of granular beds increases parabolically with the immersion depth. Translational drag increases linearly with the cylinder diameter, and the rotational drag increases with the square of the cylinder's diameter. It should, however, be pointed out that for some studies the particle size had an effect and was taken into account [1,2]; whereas, for other studies the particle size had only a negligible affect [4,5,11,12].

Rotating vanes have been used to characterize the rheological properties of many complex fluids, because the geometry prevents slipping of the sidewalls against the sheared material, which can occur for rotating cylinders [18]. Vanes have been used to measure the yield stresses [19,20], and thixotropic behavior [21] of fluids. DaCruz *et al.* [22] employed vanes to measure the yield stresses and thixotropy of granular matter and make comparisons with the rheology of foams and emulsions.

In this study we perform granular drag experiments with vanes rotating in beds of monodisperse glass beads using a different rheological procedure. We investigate the dependence of the rotational drag on the immersion depth, the vane dimensions and the bead diameter; in Sec. IV we show scaling behavior that is an extension of the continuum theories for rotating vanes. Moreover, our rheological procedure also

*Electronic address: skoehler@physics.emory.edu

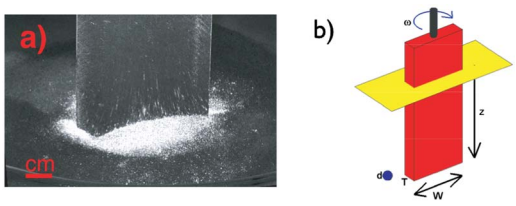

FIG. 1. (Color online) (a) Vane rotating at 0.1 rad/s in bed of 0.5 mm glass beads. The image brightness is a measure of the disturbance caused by rotation. (b) Schematic of vane immersed within the granular medium.

measures the lift force, which is the vertical force on the rotating vane, and in Sec. V we show its scaling behavior.

II. EXPERIMENTAL PROCEDURE

Experiments were performed using an AR2000 rheometer by TA instruments, which simultaneously measures the normal force and torque with a dynamical range of five decades. The shearing geometries were vanes of different width and thickness that were partially immersed in beds of monodisperse glass beads. Figure 1(a) shows the disturbance of the surface of the glass beads caused by slow rotation of a vane, which is localized about the vane. Figure 1(b) shows the experimental configuration, where the vane is partially immersed to depth z in a bed of monodisperse glass beads of diameter d. Six different vane geometries were used with widths ranging from 6 to 51 mm, thicknesses varying from 0.5 to 13 mm and aspect ratios T/W varying from 1/40 to 1/2. Two of the geometries were glass, and the rest were aluminum—there were no discernible differences in the results. Four different sizes of glass beads were used with diameters 0.5, 0.9, 2, and 5 mm. (In the experiments reported here the surfaces were smooth; however, wrapping the vanes with sandpaper did not alter the resistance.) Thus for the combination of the largest glass beads and smallest vanes the system granularity, defined in terms of the ratio of the bead diameter to vane width, was close to unity.

We developed a rheological procedure to measure the drag and lift forces on vane geometries for a range of immersions depths $0 \leq z \leq 75$ mm, by simultaneously changing the vertical position of the geometry and maintaining a set angular velocity. The beads were in a large Pyrex glass dish with a diameter of 18.7 cm and a vertical height of 10 cm. Prior to each experiment, the glass beads were manually stirred and then leveled to produce a flat surface. Then the intruder was immersed into the granular bed to a depth of $z \approx 65$ mm. The rheometer presheared the beads for one minute at this immersion depth with an angular velocity $\omega = 2$ rad/s. During the experiment the angular velocity was held at $\omega = 2$ rad/s, and the intruder was *slowly* withdrawn at a rate of 25 μm/s out of the bed. Then the vane was *slowly* immersed back into the granular bed at the same rate of 25 μm/s, until it reached the initial immersion depth. The vertical motion of the intruder was sufficiently slow that the torque and vertical force measurements were the same whether the vane was moving upward or downward. We verified that the experiments were in the quasistatic regime, by checking that increasing and decreasing the shearing rates did not alter the torques and forces.

The immersion depth z of the vane was determined from the torque measurements. As long as a portion of the intruder is inside the granular bed a torque is registered, and when it is outside the granular bed the torque drops to zero. The transition between zero and nonzero torque locates the top of the surface of the granular bed, i.e., $z=0$. Repeating the experiments showed good reproducibility of the torque and vertical force to within 5% and 15%, respectively. We verified that this continuous procedure yielded the same results as for a discrete procedure, where the geometry is rotated at a fixed immersion depth. So although the experiments may appear slow, because their duration typically was 90 min, in fact they are significantly faster and more accurate than using the discrete procedure at several different immersion depths.

III. RESULTS

Measurements show that the torque and lift on the rotating vanes increase with the bead size, immersion depth, vane width, and vane thickness. Figure 2 shows the dependence of the torque and lift plotted against an effective immersion depth $z+d/2$. Results for three vanes rotating in the $d=0.5$ and 5 mm diameter glass beads are shown. It should be noted that the rotational drag forces and the vertical lift forces are comparable, because the distance of the vane's outer edge to the center of rotation is on the order of centimeters. As expected, the relative fluctuations of the torque and lift force increase with the granularity of the system, i.e., as the bead size becomes large relative to the dimensions of the vane. Furthermore, the fluctuations of the lift are about

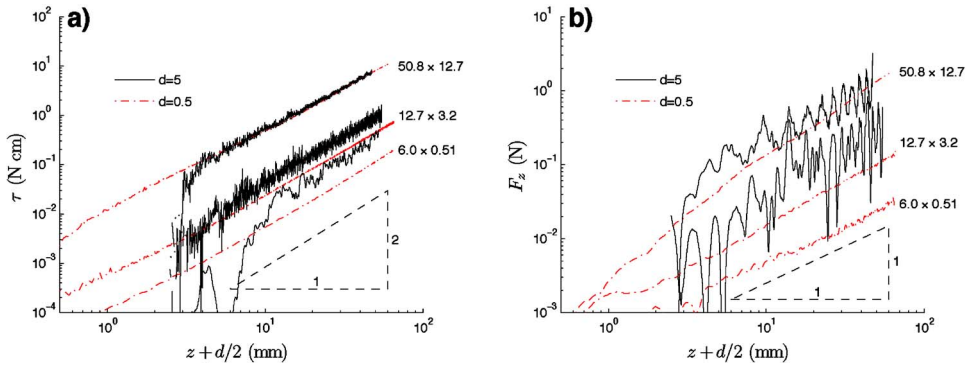

FIG. 2. (Color online) Drag and lift on vanes of different dimensions $W \times T$ immersed into two granular beds, with bead diameter $d=0.5$, 5 mm. (a) Torque plotted against the effective immersion depth $z+0.5d$. For the two smallest geometries, the data have been smoothed. (b) Lift plotted against the effective immersion depth, where the data have been smoothed.

TABLE I. Best-fit parameters to the torque given in Eq. (1), in order of increasing complexity. The effective vane length is D and the effective vane immersion depth is Z. Note that z is the nominal immersion depth, as described in the experimental procedure. Entries containing "NA" indicate that the corresponding term is not applicable and has been omitted.

D	Z	c	δ	ζ	χ^2
W	z	0.83	NA	2.07	0.084
$\sqrt{W^2+T^2}$	z	0.76	NA	2.10	0.080
$W+2\delta d$	$z+\delta d$	0.69	0.46	1.96	0.035
$\sqrt{W^2+T^2}+2\delta d$	$z+\delta d$	0.62	0.52	1.97	0.024

an order of magnitude greater than the torque fluctuations. In fact, the fluctuations of the lift for the largest beads and smallest geometries were so large, that the corresponding data set was not included in Fig. 2(b).

The choice of the effective immersion depth $z+d/2$ for the abscissa of Fig. 2 can be justified with a simple geometric argument. A rotating vane inserted at nominal depth z will be in physical contact with a volume of granular medium that is one bead size deeper than the vane; therefore, the resulting sheared region for larger beads extends deeper than for smaller beads. Thus the effective immersion depth is about one bead radius deeper than the nominal immersion depth. Plots of the torque support this assumption by showing a power-law trend over the entire range, when the immersion depth is increased by a bead radius. As seen from the plots, the torque measurements have a parabolic dependence on the immersion depth, which is the trend observed in previous studies [4,11]—see Eq. (1). Without including the bead radius, the results for the smallest beads are relatively unaffected; however, the torque measurements for the largest beads deviate from a straight line for small immersion depths $z \leq 10$ mm. So inclusion of the bead dimensions for the effective immersion depth preserves the parabolic trends for the torque at small depths and is based upon an intuitive geometric argument.

The torque and lift forces increase with the bead size, and is most pronounced when the smallest vane is combined with the largest beads. For example, increasing the bead size from $d \lesssim W/10$ to $d \sim W$ increases the torque roughly be a factor of 4. A similar trend is observed for the lift forces; increasing the bead size from $d \lesssim W/10$ to $d \sim W$ increases the torque roughly be a factor of 2.

IV. SCALING OF THE ROTATIONAL DRAG

Previous experiments performed with rotating cylinders in granular beds have been interpreted using continuum approaches. Tardos *et al.* used a critical-state soils approach [11,12] and found that the granular pressure increases linearly with depth beneath the surface, $N \sim \rho g z$. Using Amanton's friction law, the frictional stress acting on the side of the cylinder at a certain depth is $\sigma \sim \mu \rho g z$, where μ is the dynamic friction coefficient. Thus, the torque on a cylinder immersed to depth Z is a surface integral of the shear stress over the side, which can be written as a scaling relationship

$$\frac{\tau}{\rho g D^4} = c\left(\frac{Z}{D}\right)^{\zeta}, \tag{1}$$

with prefactor $c=\mu\pi/4$ and immersion depth exponent $\zeta=2$. This result was in good agreement with the experiments they performed on powders [11]. Another continuum approach for rotating cylinders based upon hydrodynamics was developed by Losert *et al.* [16] and Bocquet *et al.* [17]. They developed an expression for the effective viscosity, and in the limit of slow flows obtained results similar to those of Tardos *et al.* (although the prefactor was not explicitly determined).

To understand the rotational drag measurements we use a scaling approach similar to Eq. (1) that was developed using continuum theories. Since the experiments clearly show that the drag increases by increasing the ratio of particle diameter to vane dimensions, T and W, the bead size can not be neglected. We choose to incorporate the finite bead size using effective lengths for the immersion depth and the vane diameter, which are augmented by the particle size. This can be justified by considering the nominal volume of particles that touches a thin vane during a rotation, which is a cylinder of width $W+2\delta d$, and depth $Z+d$. Thus we choose $Z+\delta d$ for the effective immersion depth, $W+2\delta d$ for the effective width, and $T+2\delta d$ for the effective thickness. We expect δ to be a correction of order 1. Since the vane has a finite thickness, which varies from much smaller than the width to half the width, it is reasonable to expect that the vane's thickness affects the torque, and enters into the geometrical length scale D of Eq. (1). In Table I, different analytical forms for the vane's effective length scale and immersion depth are given. For each formulation parameters were determined by minimizing the corresponding χ^2 error. Since log-log plots are used, and power laws are expected, the fitting error is given in terms of the logarithmic deviations between the measured values m_i, and the predicted values p_i: $\chi^2 = \Sigma_i^N [\ln(m_i/p_i)]^2/N$.

Table I gives the parameters c, D, Z, ζ, and the χ^2 error from the best fit for four different formulations of Eq. (1). The first row gives the best fit for the simplest relationship for the torque $\tau=0.83\rho g W^{1.93} z^{2.07}$, which neglects the vane thickness and bead size, and also gives the largest fitting error. The vane thickness can naturally be incorporated by using the vane "diameter," which we define as $\sqrt{W^2+T^2}$. The second row of the table shows that this improves the fit slightly. The best fit, corresponding to the smallest χ^2 error, involves the effective vane diameter and immersion depth. Good agreement with the rescaled data using this formulation is shown by the master plot of the rescaled torque versus the rescaled immersion depth in Fig. 3(a). Figure 3(b) shows how the fitting error varies with δ and ζ.

The best fit for the torque, which involves the vane diameter and effective immersion depths, is in good agreement with the scaling given for rotational drag on cylinders given by Eq. (1), which was determined from continuum approaches [11,12,16,17]. The fitted exponent is $\zeta=1.97\pm0.2$, and is in good agreement with the exponent $\zeta=2$, which has

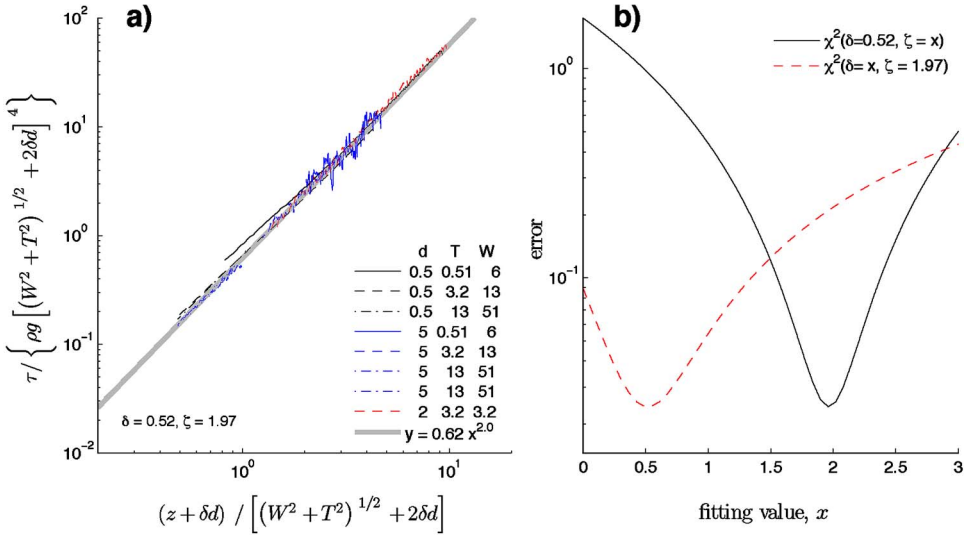

FIG. 3. (Color online) (a) Rescaled plot of the torque dependence on the immersion depth, for three vanes, including the smallest and largest vanes, and the smallest and largest beads. The thick, solid gray line shows the best fit to a power law given by Eq. (1) (the last row of Table I), where the vane diameter is used and the finite bead size is included. (b) The dependence of the mean square fitting error on the three fitting parameters—see the text.

been calculated using continuum approaches. The vane diameter is augmented by $1.24d$, and the immersion depth is augmented by $0.62d$, which is in agreement with the simple geometrical argument given above. Finally, we compare the prefactor c from the experiments with the theory [11]. The friction coefficient for smooth glass beads is $\mu \approx 0.36$, which leads to a theoretical prediction of $c \approx 0.3$ for rotating cylinders and is about half of the experimentally determined value for vanes. This is not surprising because unlike vanes, cylinders only tangentially shear beads; whereas beads at the advancing sides of vanes will also be pushed. Thus, a surface integral of the stresses acting on the vanes is a combination of shear stresses as well as normal stresses.

V. SCALING OF THE VERTICAL LIFT

Interpreting the lift forces acting on rotating vanes is far more challenging in many ways. Neither Bocquet *et al.* nor Tardos *et al.* deal with the lift forces in their experiments involving rotating cylinders [11,17]. Second, the scatter in the normal forces is about an order of magnitude larger than for the torques. Third, for the largest beads the normal forces show an oscillation that depends on immersion depth—see Fig. 2(a). In order to deal with the latter two complications, we smooth the data and omit the largest beads from the fitting and error analysis.

The continuum approaches state that the granular pressure on the sides of the cylinders is hydrostatic in nature. The close agreement with the vane experiments indicates that the granular pressure on the sides of the vanes should also be hydrostatic in nature. One would naively expect that the lift force acting on the bottom of the rotating vane is proportional to the area of the vane bottom and the granular pressure: $F_z \sim \rho g z W T$. The best fit using the naive estimate is $F_z = 3.5 \rho g W T z$, which, however, does not follow the trends of the data and has a large error $\chi^2 = 0.78$. Thus we formulate a more general scaling ansatz for the lift force

$$\frac{F_z}{\rho g \ell^3} = c A^{\kappa} \left(\frac{Z}{\ell} \right)^{\lambda}, \tag{2}$$

where ℓ is the length scale for the lift force, and A is the geometry's aspect ratio ($A = T/W \leq 1$). The exponents are κ for the aspect ratio, and λ for the effective immersion depth Z. The length scale of the lift force does not have to be the vane diameter; indeed given the above estimate, $\ell = W$, $A = T/W$, $\kappa = 1$, and $\lambda = 1$.

Table II shows six formulations for the lift force in order of increasing complexity of the effective vane dimensions. The first row is a simple estimate, which neglects the vane's thickness and the bead size, and has the largest error (but still performs much better than the naive estimate). A slight improvement is seen in the second row, where the vane's thickness has been incorporated by using the vane diameter. A further improvement is seen in the fourth row, when the fi-

TABLE II. Table of the best-fit parameters to the lift force given by Eq. (2), in order of decreasing fitting error.

ℓ	Z	c	δ	A	κ	λ	χ^2
W	z	1.27	NA	NA	NA	1.36	0.31
$\sqrt{W^2+T^2}$	z	0.48	NA	NA	NA	1.36	0.26
$W+2\delta d$	$z+\delta d$	0.92	0.63	NA	NA	1.27	0.29
$\sqrt{W^2+T^2}+2\delta d$	$z+\delta d$	0.42	0.70	NA	NA	1.25	0.23
$\sqrt{W^2+T^2}+2\delta d$	$z+\delta d$	0.87	0.38	$(T+2\delta d)/(W+2\delta d)$	0.44	1.29	0.10
$W+2\delta d$	$z+\delta d$	1.07	0.33	$(T+2\delta d)/(W+2\delta d)$	0.51	1.28	0.10

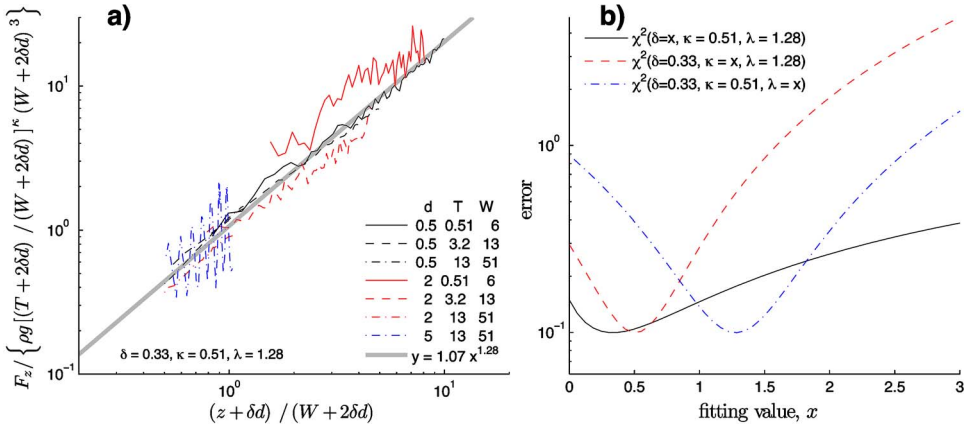

FIG. 4. (Color online) (a) Rescaled plot of the lift force dependence on the immersion depth, for three vanes, including the smallest and largest vanes. The thick, solid gray line shows the best fit to the power law given by Eq. (2) and the last row of Table II. (b) The dependence of the mean square fitting error on the three fitting parameters δ, κ, and λ.

nite bead size is included in terms of effective vane diameter and aspect ratio. The justification for working with an effective aspect ratio $(T+2\delta d)/(W+2\delta d)$ is that we expect a lift force acting on the vane even in the limit of very thin vanes, because beads about the vane's bottom will be pushed down by the bottom edge as the vane rotates. The last two rows show the best results, when the bead size, aspect ratio, and immersion depth are used. It should be noted that for all of the trial functions the depth dependence of the lift force is supralinear, and has the trend $F_z \sim Z^{1.3\pm0.1}$.

Figure 4(a) is a rescaled plot of the data using the parameters from the last row of Table II. Although the $d=5$ mm beads were omitted from the fitting analysis, Fig. 4(a) shows that the normal forces from shearing $d=5$ mm beads follow the same trends as for smaller beads. The sensitivity of the fitting error on the parameters δ, κ, λ is plotted in Fig. 4(b).

The lift on the rotating vane is due to the pressure acting on the bottom surface of the vane, which experiments show increase in a supralinear fashion, $N \sim z^{1.3}$. Furthermore, the pressure on the bottom of the rotating vane is not uniformly distributed, because the lift increases sublinearly with the vane thickness $F_z \sim T^{1/2}$. We conjecture that the pressure at the leading edge of the vane is greatest, because the shearing causes dilation of the regions in front of the leading edge; conversely, behind the leading edge the dilated regions collapse. In this fashion, the flow of beads along the vane's bottom may resemble boundary layer theory for viscous fluids [23].

VI. CONCLUSIONS

The torque on vanes rotating in glass beads follows the same power-law behavior as cylinders [11,12,16,17], when the vane diameter is used and finite bead size effects are included. The only difference is that the torque on vanes is twice that of cylinders with an equivalent diameter. We attribute the difference in prefactor between vanes and cylinders to two effects. First, the sides of a vane actually push beads; whereas for rotating cylinders, the sides are only shearing the beads. Second, as can be seen from Fig. 1(a), the shearing zone for a vane extends over tens of bead diameters, which is much greater than the shearing zone commonly observed for rotating cylinders (about ten bead diameters) [17].

The lift forces have very different dynamics from the torques. Unlike the torque, the lift strongly depends on the effective aspect ratio, and experiments indicate the dependence $F_z \sim A^{1/2}$. Furthermore, the relative fluctuations of the forces on the bottom of the vane are far greater than those on its sides. Moreover, we deduce that pressure on the bottom of the vane is not hydrostatic, but has a supralinear immersion depth dependence $F_z \sim z^{1.3}$ and also is not uniformly distributed along the bottom face. A similar depth dependence has been observed for intruders slowly plunging into beds of glass beads [10]. Although the rotating vane is not plunging into the granular bed, the shearing causes a dilatational flow, where locally the beads are moving upward toward the free surface. Thus, the granular flow about the vane's bottom surface resembles that for plunging intruders. The similarity extends to the force dependence on the width and thickness of the intruder; in both cases the lift depends linearly on the longest dimension $(F_z \sim W)$ and sublinearly on the shorter dimension $(F_z \sim T^{1/2})$. However, the prefactor for plunging is about an order of magnitude greater than that for rotation, which may result from loosening of the granular pack during the shearing process.

By augmenting the vane's dimensions by a bead diameter, the experimentally determined power-law trends of both the torque and lift force are preserved even when the beads are comparable in size to the vane. This experimentally justifies extending continuum approaches for mean, time-averaged forces to very granular systems.

Based upon these experiments, we formulate the following picture of the forces along the sides and bottom of the rotating vane. Along the sides of the rotating vanes the granular pressure is hydrostatic, i.e., increases linearly with depth. On the bottom surface of the rotating vane the average pressure increases supralinearly with depth, and is not uniformly distributed. We conjecture that the pressure is greatest at the leading edge and diminishes in the direction of the flow.

ACKNOWLEDGMENTS

The authors thank F. Family for suggestions and the Emory machine shop for manufacturing the vanes.

[1] D. Chehata, R. Zenit, and C. R. Wassgren, Phys. Fluids **15**, 1622 (2003).
[2] C. R. Wassgren, J. A. Cordova, R. Zenit, and A. Karion, Phys. Fluids **15**, 3318 (2003).
[3] K. Wieghardt, Mech. Res. Commun. **1**, 3 (1974).
[4] R. Albert, M. A. Pfeifer, A. L. Barabasi, and P. Schiffer, Phys. Rev. Lett. **82**, 205 (1999).
[5] I. Albert, J. G. Sample, A. J. Morss, S. Rajagopalan, A. L. Barabasi, and P. Schiffer, Phys. Rev. E **64**, 061303 (2001).
[6] I. Albert, P. Tegzes, R. Albert, J. G. Sample, A. L. Barabasi, T. Vicsek, B. Kahng, and P. Schiffer, Phys. Rev. E **64**, 031307 (2001).
[7] M. B. Stone, R. Barry, D. P. Bernstein, M. D. Pelc, Y. K. Tsui, and P. Schiffer, Phys. Rev. E **70**, 041301 (2004).
[8] F. Zhou, S. G. Advani, and E. D. Wetzel, Phys. Rev. E **69**, 061306 (2004).
[9] F. Zhou, S. G. Advani, and E. D. Wetzel, Phys. Rev. E **71**, 061304 (2005).
[10] G. Hill, S. Yeung, and S. A. Koehler, Europhys. Lett. **72**, 137 (2005).
[11] G. I. Tardos, M. I. Khan, and D. G. Schaeffer, Phys. Fluids **10**, 335 (1998).
[12] G. I. Tardos, S. McNamara, and I. Talu, Powder Technol. **131**, 23 (2003).
[13] R. C. Rowe and G. R. Sadeghnejad, Int. J. Pharm. **38**, 227 229 (1987).
[14] A. Dareliusa, A. Rasmusona, I. N. Björn, and S. Folestad, Powder Technol. **160**, 209 (2005).
[15] The drag forces on shallow granular beds of monodisperse glass beads are not very sensitive to the initial conditions. In plunging and withdrawal experiments the drag forces did not change for successive experiments [10]. P. Schiffer (private communication) reports that the drag forces reported in [4,5] were unaffected by the presence of a "rake" in front of the moving intruder.
[16] W. Losert, L. Bocquet, T. C. Lubensky, and J. P. Gollub, Phys. Rev. Lett. **85**, 1428 (2000).
[17] L. Bocquet, W. Losert, D. Schalk, T. C. Lubensky, and J. P. Gollub, Phys. Rev. E **65**, 011307 (2001).
[18] A. S. Yoshimura, R. K. Prudhomme, H. M. Princen, and A. D. Kiss, J. Rheol. **31**, 699 (1987).
[19] M. Keentok, Rheol. Acta **21**, 325 (1982).
[20] N. J. Alderman, G. H. Meeten, and J. D. Sherwood, J. Non-Newtonian Fluid Mech. **39**, 291 (1991).
[21] P. Coussot, Q. D. Nguyen, H. T. Huynh, and D. Bonn, J. Rheol. **46**, 573 (2002).
[22] F. DaCruz, F. Chevoir, D. Bonn, and P. Coussot, Phys. Rev. E **66**, 051305 (2002).
[23] G. K. Batchelor, *An Introduction to Fluid Dynamics* (Cambridge University Press, Cambridge, U.K., 1973).